Fluid Phase Equilibria 576 (2024) 113935

Contents lists available at ScienceDirect

Fluid Phase Equilibria

journal homepage: www.sciencedirect.com/journal/fluid-phase-equilibria

Estimation of Flory–Huggins interaction parameters and miscibility gaps in poly(sodium 4-styrenesulfonate) - water - 1,4-butanediol mixtures via linearized cloud point curve correlations

Rinsha Padmarajan, Sreeram K. Kalpathy *

Department of Metallurgical and Materials Engineering, Indian Institute of Technology Madras, Chennai 600036, India

ARTICLE INFO

Keywords:
Flory–Huggins theory
Poly(sodium 4-styrenesulphonate)
Cloud point
Chi parameter
Non-solvent induced phase separation

ABSTRACT

The phase behavior of poly(sodium 4-styrenesulfonate) (NaPSS) – water system in the presence of a non-solvent 1,4-butanediol was investigated at 25 °C and 50 °C using cloud point titration method, combined with linearized cloud point (LCP) correlation. Using a limited number of experimental cloud points, the solubility curve for the entire composition range in the ternary system was determined numerically by extrapolation, with the help of LCP fitting parameters. The Flory Huggins (FH) interaction parameters (χ) of the constituent binary systems were estimated through a mathematical model, built using a combination of LCP fit and an extended FH equation for the Gibbs energy of mixing. The model accounts for entropy of mixing of counterions as well as the electrostatic interaction energy based on Manning's theory. The χ parameters thus determined are found to be in agreement with the expectations of favorable NaPSS–water interactions and unfavorable NaPSS–1,4-butanediol interactions. Analysis of the individual contributions to Gibbs energy of mixing reveals that bulk of the contribution arises from FH entropy and FH enthalpy, while the counterion entropy and electrostatic energy are rather small in the present system.

1. Introduction

Understanding phase equilibria is critical for polymer processing, which often occurs in a solution state. The prediction of miscibility gaps, or the identification of composition ranges over which a homogeneous mixture phase separates into multiple mixed phases [1,2] is crucial to several applications involving polymers and complex fluids. Examples include controlled drug delivery [3,4], polymer membrane fabrication [5,6] fibre spinning [7], energy devices [8], fluid equilibration in oilfield reservoirs [9], and extraction processes [10,11]. Miscibility gaps in polymer-solvent systems or polymer-polymer blends are typically identified via temperature-composition plots, wherein thermodynamically stable, metastable, and unstable regions can be demarcated. The phase behavior however may differ substantially. There can be an upper critical solution temperature (UCST), lower critical solution temperature (LCST), closed loop immiscibility curve, hour glass shaped phase boundaries [12] etc. These complexities may prevent exclusive experimental determination of phase behavior of polymer systems. This emphasizes the need for various predictive thermodynamic models to determine phase diagrams of polymer mixtures.

Numerous thermodynamic models for polymer mixtures have been proposed over the last few decades. These include the classical Flory–Huggins theory [13–15], Sanchez–Lacombe equation of state theory [16], UNIFAC-FV, SAFT [17] etc. Although sophisticated models can provide more accurate thermodynamic descriptions, the classical Flory–Huggins (FH) theory still retains popularity due to its conceptual and mathematical simplicity. The FH interaction parameter χ, which appears in the enthalpic contribution to mixing, is a numerical indicator of polymer-solvent or polymer-polymer molecular energetic interactions. Often, the value of χ is a benchmark for classifying solvents as good, poor or theta solvents. Besides, χ can be used to estimate many other thermodynamic properties of polymer-based mixtures [18]. Typical methods to estimate χ are Hansen solubility parameter-based approach [19,20], osmotic pressure measurements [21,22], inverse gas chromatography [23], light scattering [24,25], and calorimetric measurements [26].

Polyelectrolyte systems have additional complexities in comparison to regular polymer systems. Factors like electrostatic interactions resulting from charges on the chains and counterions, as well as the ordering tendency of ions will affect the Gibbs energy. Moreover, complex formation is likely in polyelectrolyte blends. These intricacies have prompted the use of advanced frameworks like PRISM theory [27] and self-consistent field approach [28] in polyelectrolyte solution thermodynamics. Yet, the classical FH theory and its simple extensions

* Corresponding author.
E-mail address: sreeram@iitm.ac.in (S.K. Kalpathy).

https://doi.org/10.1016/j.fluid.2023.113935
Received 4 May 2023; Received in revised form 10 August 2023; Accepted 25 August 2023
Available online 28 August 2023

have been routinely in use until date to understand phase behavior of such systems. Safronov et al. [26] determined the FH binary interaction parameter χ in polyelectrolyte hydrogels based on poly(acrylic) acid and poly(methacrylic) acid with different counterions using osmotic pressure measurements. They estimated the enthalpic and entropic contributions to χ and concluded that the overall χ value is largely unaffected by the nature of counterions, though the individual contributions might be affected. Lopes et al. [29] estimated the interaction parameter in the natural polymer mixture of silk fibroin and sodium alginate using the plain FH model. Despite its simplicity, the model was able to achieve acceptable correlations with experimental observations. Kwon et al. [30] also based their phase equilibria theory of polyelectrolyte blends on the classical FH theory, but with a couple of additional terms in the Gibbs energy to account for counterion entropic contribution and electrostatic coupling. Therefore, the plain FH model can be considered as a reasonable starting point for more elaborate treatments to describe inter-system interactions. Besides, in systems with high concentration (~10 wt%) of polyelectrolyte, there will be significant screening of electrostatic interactions, and the magnitude of Gibbs energy terms that depend on ionic composition will be negligible [31].

Poly (sodium 4-styrenesulfonate) (NaPSS) is an industrially and medically useful, water-soluble, anionic polyelectrolyte. It is a macromolecule with sulfonate-substituted negatively charged aromatic rings in the vinylic positions of the carbon–carbon backbone chain, with sodium as the positively charged counterion. It is reported to be a key ingredient in the drugs used for treatment of hyperkalemia disorder [32–35]. NaPSS is also used as flocculant, and in the development of controlled drug delivery membranes [36–38]. Another interesting application of NaPSS is its employment as a charge balancing dopant for enhancing the aqueous solubility of conducting polymers like poly(3,4-ethylenedioxythiophene) (PEDOT) [39,40]. These diverse applications of NaPSS entail the understanding of its phase behavior in aqueous environments, which are less investigated in published literature. In this work, we investigate the phase equilibria of NaPSS – water system in the presence of a third component 1,4-butanediol, specifically focussing on cloud point curves in the ternary system. 1,4-butanediol is an organic solvent widely used in the manufacture and processing of several polymers [41]. Here, we employ it as a non-solvent in the NaPSS – water mixture to engender phase separation.

A simple, effective, experimental method for gaining insights into polymer phase equilibra is the determination of the "cloud point" curve, i.e., the threshold compositions at the onset of polymer demixing, by titrating a polymer-solvent mixture against a non-solvent [42,43]. When a homogeneous solution of polymer in the solvent is titrated against a minimum critical quantity of the non-solvent, immiscibility is induced, which is visually manifested as turbidity or cloudiness in the solution. The cloud point information thus obtained provides the "solubility curve" of the system [44]. Furthermore, if a few cloud points of such a ternary system are determined by varying the solvent : non-solvent ratio, the available set of data points can be extrapolated to find the solubility curve over the entire composition range with the help of linearized cloud point (LCP) curve correlation technique [45]. Besides, the cloud point data can be used to estimate the binary interaction parameters of the constituents present, using FH-type models.

In this work, we pursue the determination of cloud points in NaPSS–water–1,4-butanediol ternary system through the combination of non-solvent titration and LCP correlation. We also estimate the FH binary interaction parameters between NaPSS and water, as well as NaPSS and 1,4-butanediol using a suitable extension of the FH model. Section 2 provides the required theoretical background relevant to our system, as well as the mathematical procedure of LCP method. Section 3 details the experimental procedure used. In Section 4, we describe the results, beginning with cloud point curves from experimental data (Section 4.1), followed by estimation of FH interaction parameters (Section 4.2) and the various contributions to Gibbs energy in this system. Section 5 provides the concluding remarks.

2. Theoretical background

2.1. Relevant extension of the Flory–Huggins model

The Flory–Huggins theory [13–15] is a natural extension of regular solution model [46], that assumes a lattice arrangement of the constituent polymers and/or solvent molecules to estimate the entropy and enthalpy of mixing. For a ternary mixture consisting of uncharged components (1,2,3), with their molar volumes V in the order $V_3 > V_1 > V_2$, the total Gibbs energy of mixing $\Delta_{\text{mix}}G$ is given by [47]:

$$\frac{\Delta_{\text{mix}}G}{RT} = n_1 \ln \Phi_1 + n_2 \ln \Phi_2 + n_3 \ln \Phi_3 + n_2\Phi_1\chi_{12} + +n_2\Phi_3\chi_{23} + +n_1\Phi_3\chi_{13}, \tag{1}$$

where R is the ideal gas constant, T is the temperature, χ_{ij} $(i, j = 1,2,3)$ are interaction parameters between each $i-j$ pair of components, n_i and Φ_i denote the number of moles and volume fraction respectively of the component i. For simplicity, the ternary interaction parameter χ_{ijk} is typically ignored. The volume fraction of component i can be related to its number of moles through molar volumes, by the expression:

$$\Phi_i = \frac{n_i V_i}{\sum_{i=1}^{3} n_i V_i}. \tag{2}$$

The first three terms on the right hand side (RHS) of Eq. (1) account for the combinatorial entropy of mixing, and the last three terms represent the enthalpy of mixing. The temperature-dependent F-H interaction parameter χ_{ij} between each $i - j$ pair is defined as:

$$\chi_{ij} = \frac{z\Delta w_{ij}}{k_B T}, \tag{3}$$

where z is the lattice coordination number, k_B is the Boltzmann constant, and Δw is the change in internal energy brought about by one pair of $i - j$ molecular interaction. In other words, χ_{ij} in a polymer-solvent system may be conceptualized as the fraction of $k_B T$ energy required to bring one isolated molecule each of a polymer and solvent into the solution lattice. Thus, it is a parameter that allows for the quantification of affinity between molecules of i and j.

If the polymer of relevance is a polyelectrolyte (such as NaPSS in our study), then additional terms for counterion entropy and electrostatic interactions need to be included in the RHS of Eq. (1). Two notable approaches have been proposed in the literature for counterion entropy. One way to account for it is by considering the counterions as an additional species [31,48,49], through a term of the type $n_4 \ln \Phi_4$ in (1), with the index 4 denoting counterions. An alternative way, as suggested by Khokhlov and Nyrkova [50], would be to include the entropic contributions of free counterions within the polymer term itself in Eq. (1). In other words, if the index 3 in Eq. (1) denotes the charged polymer, then the third term on the RHS of (1) may be written as $n_3(1 + \alpha) \ln \Phi_3$, where α is the number of free counterions per chain of the polyelectrolyte. This approach, later termed as the "effective length approximation" by Gottschalk et al. [51], simply amounts to renormalization of the number of segments of the polymer chain occupying a lattice site. Both approaches have been shown to capture trends from experimental data reasonably well [51,52]. The value of α may be estimated from Manning's counterion condensation theory [53], which depends on factors like valence of ions, mean spacing between charged groups in the polymer, and the dielectric constant of the dissolution medium.

The long range electrostatic interactions can be accounted for through the Debye–Huckel or Manning limiting laws [53–55]. For the case of n_3 moles of a neutral polyelectrolyte containing N univalent charged groups per chain, with as many counterions, among which a fraction f are dissociated in the solvent, the electrostatic contribution to the Gibbs energy [54] is given by $\Delta G_{\text{el}}/RT = -(\xi/2) f^2 N n_3 \ln(f\Phi_3)$.

Here, ξ is the charge density parameter of the polymer from Manning theory. This electrostatic energy contribution would be added to the RHS of Eq. (1) to model the total Gibbs energy of mixing.

We note that supplementing the Gibbs energy of mixing with additional terms in a very similar manner as above is conventionally followed in the literature for modeling effects like complexation in polyelectrolyte blends and micelle formation [56,57]. For instance, in micelle formation, the Gibbs energy would contain additional terms pertaining to the interfacial energy, contribution from deformation of the polymer chains, and the entropy of mixing of polymer chains inside the micelle corona [58].

2.2. Miscibility gaps in polymer-solvent systems

It may be noted that even in multi-component systems which possess favorable mixing tendencies by virtue of a negative $\Delta_{\text{mix}}G$, existence of a single mixed phase over all compositions is not guaranteed. Miscibility gaps can arise when there are multiple local minima in $\Delta_{\text{mix}}G$ at certain compositions, causing the co-existence of multiple mixed phases. The binodal compositions separate the metastable co-existence regions from the region where a single homogeneous mixture is stable. For polymer solutions, determination of cloud point data is commonly done in the context of phase equilibria studies. However, as pointed out by Arce et al. [44], the "solubility curve" determined through cloud point data is not a true equilibrium curve. The binodal curve, on the other hand, is a system equilibrium curve, independent of the visual perception errors that may arise while distinguishing the limit between immiscibility and homogeneity in cloud point experiments.

Mathematically, the binodal phase boundaries may be determined by solving for compositions at which the chemical potentials of each component in the mixture in the co-existing phases are equal [59–61]. At equilibrium, the chemical potential of both the polymer-rich and polymer-lean phases must be equal. In other words, at the binodal point where multiple phases are in equilibrium, we should have:

$$\mu_i\Big|_{\text{phase 1}} = \mu_i\Big|_{\text{phase 2}} = \mu_i\Big|_{\text{phase 3}} \ldots\ldots, \qquad i = 1, 2, 3, \tag{4}$$

where μ_i is the chemical potential of the ith component in the mixture, given by:

$$\frac{\Delta\mu_i}{RT} = \left.\frac{\partial\left(\frac{\Delta_{\text{mix}}G}{RT}\right)}{\partial n_i}\right|_{n_j, j\neq i, T, P}, \tag{5}$$

P denoting the system pressure, and $\Delta\mu_i = \mu_i - \mu_i^0$ is the chemical potential relative to a standard reference state. On the other hand, the spinodal curve, or the phase boundary separating the unstable, phase separated region from the metastable coexistence region can be determine by solving:

$$\frac{\partial^2(\Delta_{\text{mix}}G)}{\partial n_i^2} = 0. \tag{6}$$

2.3. Linearized cloud point (LCP) curve correlation method.

Experimental determination of the cloud point in polymer solutions is often done by cooling them slowly over temperature, or by titrating a polymer-solvent mixture isothermally against a non-solvent and tracking the onset of visual turbidity [62–64]. However, since it is difficult to titrate a polymer solution at higher concentrations due to high viscosity, obtaining the complete phase boundary is experimentally challenging [65]. For the case of a ternary system involving a polymer, solvent, and non-solvent, Boom et al. [45] proposed the LCP correlation method for determining cloud point composition curves. In order to extrapolate the limited experimental cloud point data to wider range of compositions, LCP correlation method makes use of the following linear fitting expression:

$$\ln\frac{\Phi_1}{\Phi_3} = b\,\ln\frac{\Phi_2}{\Phi_3} + a, \tag{7}$$

where Φ_1, Φ_2 and Φ_3 are the volume fractions of the non-solvent, solvent and polymer respectively at a known cloud point. The slope b in the linear fit between $\ln(\Phi_1/\Phi_3)$ vs. $\ln(\Phi_2/\Phi_3)$ contains a ratio of differences between the molar volumes of the components (V_i) as in Eq. (8):

$$b = \frac{V_1 - V_3}{V_2 - V_3}. \tag{8}$$

The intercept a of the fit contains information on the Flory–Huggins interaction parameters of the constituents involved. The complete expression for a is provided in Section 4.2.2.

The cloud point information obtained from experimental measurements can be extrapolated to the entire composition range of polymer/solvent/non-solvent system, assuming that the linear fit in Eq. (7) is obeyed throughout. Given that $\Phi_1 + \Phi_2 + \Phi_3 = 1$ among which one of the Φ_i's is independent, it is possible, in principle, to determine the value of each Φ_i at a cloud point using (7). Thus the solubility curve can be plotted on a ternary phase diagram over the entire range of composition.

3. Experimental

3.1. Materials

Poly (sodium 4-styrenesulfonate) (NaPSS, average molar mass M_w = 70 kDa as per manufacturer's label, and specific gravity 0.8), and 1,4-butanediol (molar mass 90.12 Da, specific gravity 1.02) were procured from suppliers as mentioned in Table 1 and used as-received. Deionized (DI) water (specific conductance less than 1 μS cm^{-1} at 25 °C, specific gravity 1) was procured from Nice Chemicals Pvt. Ltd., India. The viscosity-averaged molar mass of NaPSS was independently measured and found to be 32.452 kDa. Details of measurement are reported in section S1 of Supplementary material.

3.2. Preparation of polymer solution

Aqueous polymer solutions of concentrations in the range of 0.08 g/ml to 0.25 g/ml NaPSS were prepared by dissolving appropriate amounts of NaPSS in DI water. The solutions were initially mixed using a digital ultrasonicator (KLDUC-2.5, KINGLAB, India), and then continuously stirred using a magnetic stirrer (TARSONS SPINOT-magnetic stirrer and hot plate-DIGITAL, MC 02, India) for 2 h at room temperature to obtain a clear homogeneous yellow solution as shown in Fig. 1(a).

3.3. Cloud point determination

A standard titration method was performed to determine the threshold amount of the non-solvent 1,4-butanediol that can be added to aqueous NaPSS until demixing is induced. The titration was performed with a 50 ml burette with 0.1 ml graduation. The non-solvent was added dropwise from the precision burette to the aqueous polymer solution contained in a beaker, under continuous magnetic stirring, as shown in Fig. 1(b). The titration experiments were performed at two different temperatures of the solution, viz. 25 °C and 50 °C. The solution temperature was fixed with the help of the temperature controller attached to the stirring plate which had a temperature uncertainty of 0.1 °C. During each titration experiment, the turbidity of the solution was monitored with the help of a turbidimeter (TU-2016, Lutron, Taiwan). The concentration of the non-solvent at which the turbidity first increased to twice that of the previous reading was declared as the cloud point composition. The liquid mixture at this point has an appearance as in Fig. 1(c). At the cloud point thus determined, it was verified that the variation in turbidity is less than 15% throughout a holding time of at least 12 h. The translucent mixture at the cloud point composition was then diluted further with the solvent

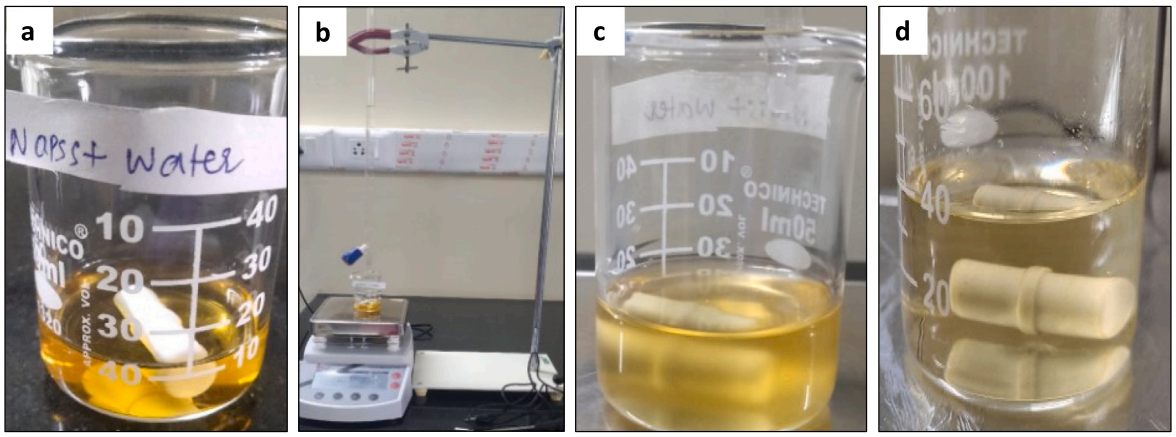

Fig. 1. (a) Homogeneous solution of NaPSS and DI water (b) Titration experiment set up (c) Visual turbidity in solution at cloud point (d) Clear solution recovered upon adding solvent (DI water) to (c).

Table 1
Specifications of chemicals used in this study.

Chemical name	CAS number	Source	Molar mass	Purity (mass%)
Poly(sodium 4-styrenesulfonate) (NaPSS in short)	25704-18-1	Alfa Aesar	70 kDa	>99.9
1,4-butanediol	110-63-4	Spectrochem Pvt. Ltd. India	90.12 Da	>99

(DI water) to form a clear solution (Fig. 1(d)), restoring a single mixed phase, and the steps of titration with 1,4-butanediol were repeated. Experiments were conducted over a limited composition range over which the viscosity of the solution was low enough to detect turbidity changes accurately. As the concentration of NaPSS or 1,4-butanediol is raised, the solution viscosity increases. Then, the re-mixing of the non-solvent upon further solvent addition to a cloud point composition mixture becomes extremely slow, rendering turbidity measurements difficult. The limited experimental data was then used for extrapolation of cloud point curve over the entire composition range using LCP curve correlation method.

4. Results and discussion

4.1. Cloud point curves from experimental data

Fig. 2(a) shows the solution turbidity measured as function of the volume of non-solvent 1,4-butanediol for a typical solution of NaPSS – water being titrated. For the specific case shown, the starting polymer solution contained 3 g NaPSS in 17 ml water (i.e. 15 wt% NaPSS in water), and the titration was performed at 25 °C. Turbidity is reported in nephelometric turbidity units (NTU), which is observed to record a sudden rise beyond ~22 ml of 1,4-butanediol, due to the onset of precipitation of excess polymer from the solution. The cloud point for this case was determined to occur at 21.7 ml non-solvent as per the criterion set in Section 3.3. Similar jumps in turbidity values were also observed for other starting concentrations and the cloud point compositions were accordingly determined. Fig. 2(b) shows the variation of turbidity values with time for the same starting composition as in Fig. 2(a), for four different volumes of 1,4-butanediol added, viz., 10 ml, 15 ml, 20 ml, and 21.7 ml. Slight transient variations in turbidity are induced due to the kinetics of mixing; however, as observed in all the four samples, the variations are within 15%, suggesting that the mixtures are kinetically stable. Given that the cloud point for this specific starting solution occurs at 21.7 ml of 1,4-butanediol, Fig. 2(b) suggests that (i) solutions containing non-solvent lesser than 21.7 ml remain as a single phase mixture within the holding timescale, and (ii) the mixture with 21.7 ml of 1,4-butanediol remains kinetically as a phase separated mixture, lending validity to the cloud point composition ascertained via the titration experiment.

Table 2
LCP fit parameters obtained for water-NaPSS-1,4-butanediol system at temperatures T = 25 °C and 50 °C.

T (°C)	Slope (b)	Intercept (a)	Correlation coefficient
25	1.437	−0.451	0.998
50	1.415	−0.495	0.991

Fig. 3 shows plots of $\ln(\Phi_1/\Phi_3)$ vs. $\ln(\Phi_2/\Phi_3)$ for (a) 25 °C and (b) 50 °C, where Φ denotes volume fraction of the components 1, 2, and 3 at the cloud point, representing the non-solvent, solvent, and polymer respectively. It is evident that the experimental data in both cases (black circles) obey a linear fit. The correlation coefficient as per linear least squares regression is found to be equal to 0.998 in (a) and 0.991 in (b), suggesting excellent goodness of fit. The linear fits obtained via least squares regression have slopes of 1.437 and 1.415, and intercepts of −0.451 and −0.495 in (a) and (b) respectively. According to Boom et al. [45] the slope of LCP fit is expected to be slightly greater than 1, which is in agreement with values reported for both the temperatures in Table 2. The theoretical value of the slope calculated using Eq. (8) and the known molar volumes (ratio of molar mass to density) is ~ 1. The variation between the computed and theoretical slopes may be attributed to the polydispersity of the polymer. The intercepts contain information about the FH interaction parameters, and will be explained in detail in Section 4.2.2.

The LCP fits were used to generate cloud point curves over the entire range of compositions by extrapolating the experimental data, as per procedure stated in Section 2.3. The extrapolated cloud point curves are shown in Fig. 4(a),(b), on the ternary phase diagram of NaPSS – water – 1,4-butanediol at 25 °C and 50 °C. The red squares represent the experimentally detected cloud points, while the solid blue lines denotes the extrapolated cloud point curve by LCP method described in Section 2.3. These curves reveal that mixtures with more concentrated NaPSS have cloud points situated towards lower concentrations of 1,4-butanediol. As expected, lesser amount of the non-solvent was required to induce the precipitation in mixtures with higher initial polymer concentration.

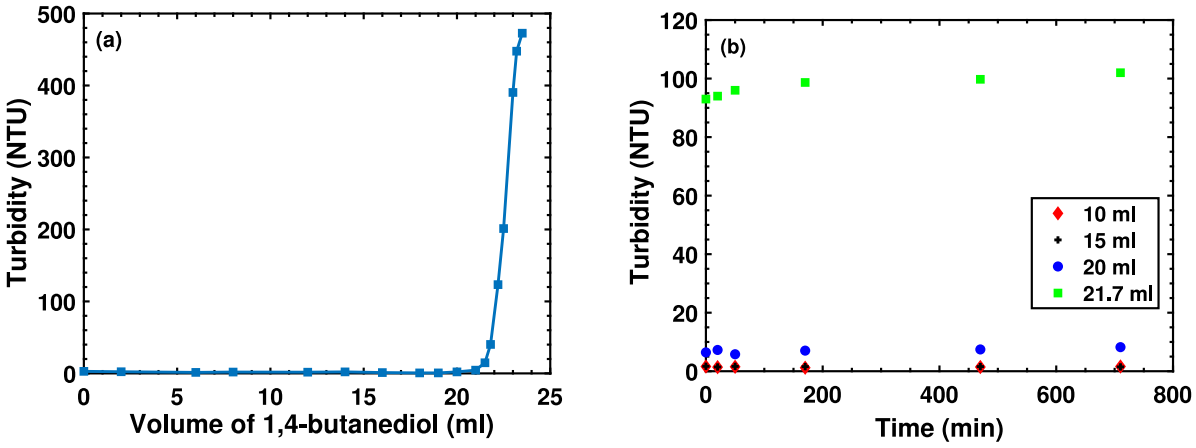

Fig. 2. Turbidity in NaPSS – water solution as a function of concentration of the non-solvent 1,4-butanediol. The starting solution had a concentration of 15 wt% NaPSS in water. (b) Turbidity variations over time for a solution containing 3 g NaPSS in 17 ml water, for four different volumes of 1,4-butanediol added during titration.

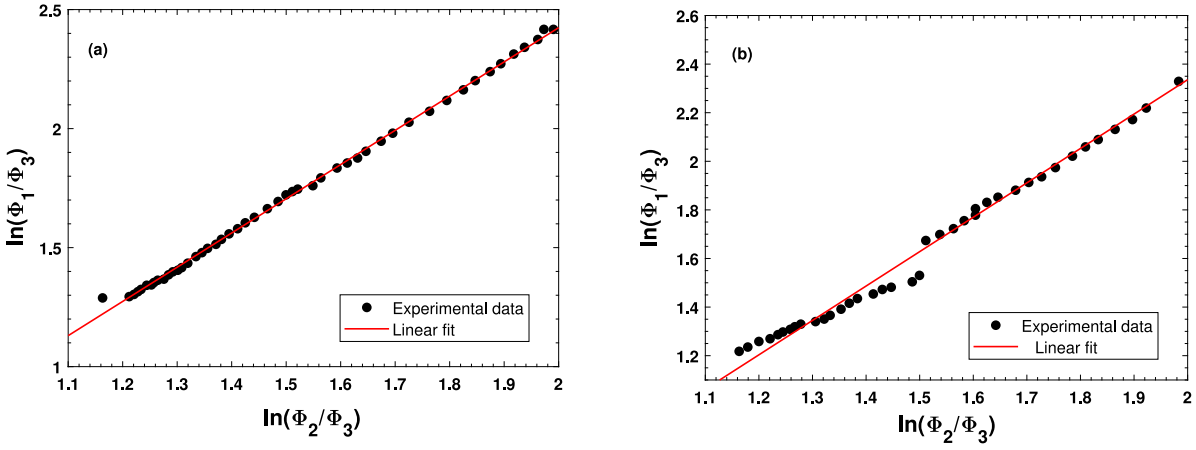

Fig. 3. The LCP fits for NaPSS/water/Butanediol system (a) at 25 °C, (b) at 50 °C.

With regard to temperature, the cloud point curves are not vastly different at 25 °C and 50 °C. Generally, miscibility in a system would improve upon heating if the additional thermal energy can compensate for the deficit in energy required for dissociation of bonds in the solvent and solute, which could not be met otherwise from the energy released during the dissolution process at the lower temperature. The temperature dependence of the interaction parameter χ would determine whether the enthalpy difference over the two temperatures is large. For the specific system in consideration, it appears that there is little tangible change over the temperature range of 25–50 °C. We also note that temperature invariance is assumed in our experiments for entropic control.

4.2. Determination of the interaction parameters

Based on the experimental results in Section 4.1 and information from the literature, the Flory–Huggins interaction parameters χ_{12}, χ_{13}, and χ_{23} were determined, where 1,2,3 denote 1,4-butanediol, water, and NaPSS respectively. Among these, χ_{12} was estimated based on enthalpy of mixing data measured previously by Nagamachi and Francesconi [66]. Its value was then used as an input for determining χ_{23} and χ_{13} based on the LCP model, to be discussed in Section 4.2.2.

4.2.1. Estimation of χ_{12}

Nagamachi and Francesconi [66] have measured the molar enthalpy of mixing $\Delta_{mix}\underline{H}$ for 1,4-butanediol - water mixtures of different mole fractions at 25 °C and 50 °C. The data is graphically presented in Fig. 5, displaying a non-monotonic variation, and suggesting that mixing is enthalpically the most favorable at mole fraction value ~ 0.35 of 1,4-butanediol. The corresponding values of χ_{12} at the different compositions were estimated using the Flory–Huggins model, i.e., $\Delta_{mix}\underline{H} = x_2\Phi_1\chi_{12}RT$, where x_2 is the mole fraction of water and Φ_1 is the volume fraction of 1,4-butanediol. The calculated values of χ_{12} are depicted in Fig. 6. The cloud point data measured in our experiments correspond to mixtures with x_2 in the range $0.17 - 0.22$, over which χ_{12} is seen to be fairly constant from Fig. 6, and can be estimated to be -0.77 and -0.47 at 25 °C and 50 °C respectively. The negative values of χ_{12} are in agreement with the idea that water and 1,4-butanediol are miscible in all proportions due the presence of hydrogen bonding between -OH groups of the alcohol and water [66].

4.2.2. Development of the LCP model and determination of χ_{23} and χ_{13}

We use the extension of Flory–Huggins theory described in Section 2.1 to build a model connecting the χ parameters with the intercept a of the LCP equation (7). The Gibbs energy of mixing $\Delta_{mix}G$ for the ternary system of species 1, 2, 3 is expressed using the extension of FH model described in Section 2.1, through a simple modification of Eq. (1):

$$\frac{\Delta_{mix}G}{RT} = n_1\ln\Phi_1 + n_2\ln\Phi_2 + n_3(1+\alpha)\ln\Phi_3 + n_2\Phi_1\chi_{12} + n_2\Phi_3\chi_{23} + n_1\Phi_3\chi_{13} - \frac{\xi}{2}f^2Nn_3\ln(f\Phi_3). \quad (9)$$

The factor α in the third term on the RHS denotes the number of free counterions per molecular chain of NaPSS, which is equal to the product fN, where N is the degree of polymerization and f is the fraction

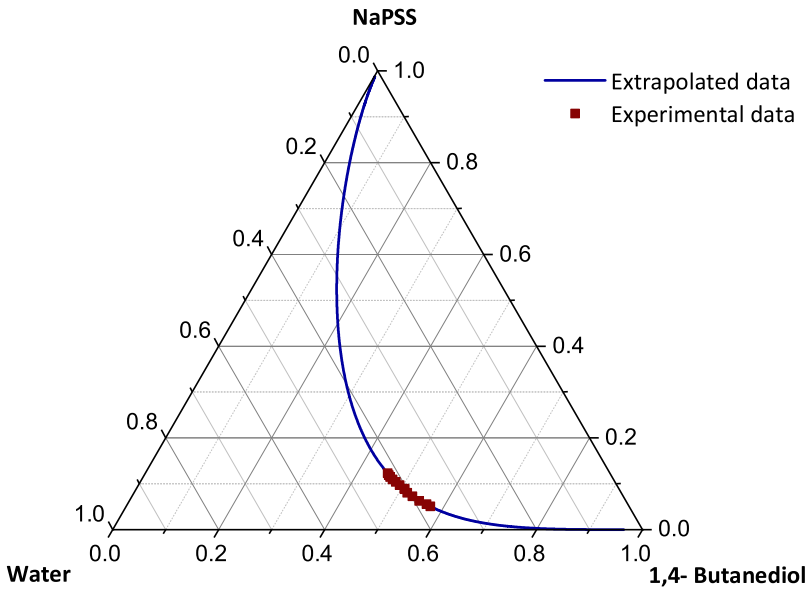

(a)

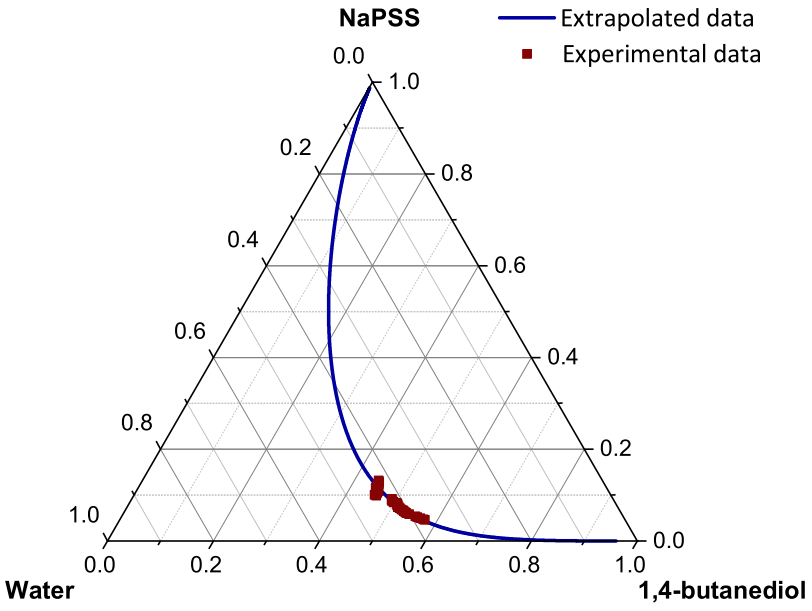

(b)

Fig. 4. The solubility curves for NaPSS/water/Butanediol system (a) at 25 °C, (b) at 50 °C. Markers represent the experimental cloud point data and the line represents the extrapolated solubility curve. Axes are in terms of volume fractions.

of free counterions. The last term on the RHS of Eq. (9) represents the electrostatic contribution. The fraction f as well as the charge density parameter ξ can be estimated based on Manning's counterion condensation theory [55]. Laatikainen et al. [67] have reported that f would be ~0.3 and ξ would be ~2.85 in aqueous solutions of fully charged vinylic polyelectrolytes such as NaPSS, containing univalent counterions, at 25 °C. The values of f and ξ are functions of temperature as well as the dielectric constant of the medium. More precise estimates for these quantities over the temperature and concentration ranges of interest are provided in Table 3.

The chemical potential of each species i ($i = 1, 2, 3$) in the mixture, relative to its standard reference state, can be found by differentiation of (9) as per Eq. (5). Note that the evaluation of $\Delta\mu_i$'s by (5) would require evaluation of the derivatives of Φ_i's with respect to n_i's. These

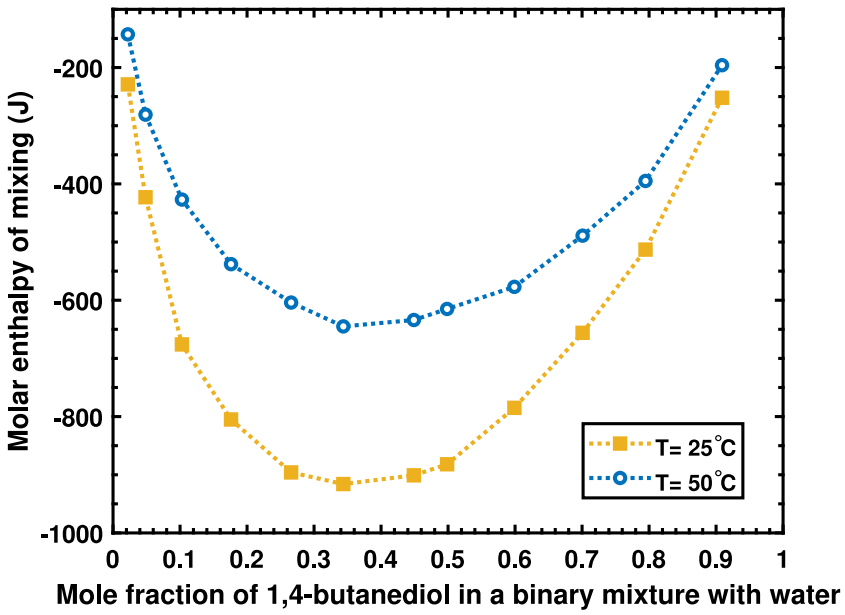

Fig. 5. Molar enthalpy of mixing for different mole fractions of 1,4-butanediol with water, based on data from Nagamachi and Francesconi [66].

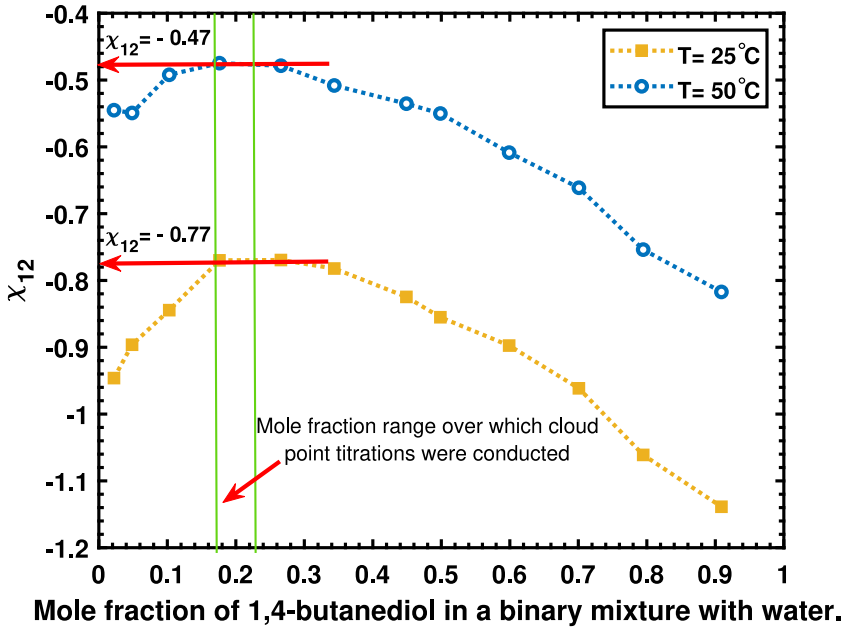

Fig. 6. Values of χ_{12} calculated using the Flory–Huggins expression for enthalpy of mixing of a binary mixture, $\Delta_{mix}\underline{H} = x_2\Phi_1\chi_{12}RT$, for values of $\Delta_{mix}\underline{H}$ plotted in Fig. 5.

expressions are provided in Appendix A. After evaluating the necessary derivatives, one obtains the following:

$$\frac{\Delta\mu_1}{RT} = \ln\Phi_1 + (\Phi_2+\Phi_3) - \frac{n_2}{n_1}\Phi_1 - \frac{n_3}{n_1}\Phi_1(1+\alpha) + \frac{n_2}{n_1}\Phi_1(\Phi_2+\Phi_3)\chi_{12} - \frac{n_2}{n_1}\Phi_1\Phi_3\chi_{23} + \Phi_3(\Phi_2+\Phi_3)\chi_{13} + \frac{\xi}{2}f^2N\frac{n_3}{n_1}\Phi_1. \quad (10)$$

$$\frac{\Delta\mu_2}{RT} = \ln\Phi_2 + (\Phi_1+\Phi_3) - \frac{n_1}{n_2}\Phi_2 - \frac{n_3}{n_2}\Phi_2(1+\alpha) + \Phi_1(\Phi_1+\Phi_3)\chi_{12} + \Phi_3(\Phi_1+\Phi_3)\chi_{23} - \frac{n_1}{n_2}\Phi_2\Phi_3\chi_{13} + \frac{\xi}{2}f^2N\frac{n_3}{n_2}\Phi_2. \quad (11)$$

$$\frac{\Delta\mu_3}{RT} = [\ln\Phi_3 + (\Phi_1+\Phi_2)](1+f) - \frac{n_1}{n_3}\Phi_3 - \frac{n_2}{n_3}\Phi_3 - \frac{n_2}{n_3}\Phi_1\Phi_3\chi_{12} + \frac{n_2}{n_3}\Phi_3(\Phi_1+\Phi_2)\chi_{23} + \frac{n_1}{n_3}\Phi_3(\Phi_1+\Phi_2)\chi_{13} - \frac{\xi}{2}f^2N(\Phi_1+\Phi_2+\ln f+\ln\Phi_3). \quad (12)$$

By virtue of (4), we know that at the phase coexistence boundaries, each component i must satisfy

$$\Delta\mu_i\big|_{\text{phase 1}} = \Delta\mu_i\big|_{\text{phase 2}}, \qquad i = 1,2,3, \quad (13)$$

where phase 1 and phase 2 are the polymer rich phase and the polymer lean phase which coexist. However, this equality also implies that any linear combination of the $\Delta\mu_i$'s must be equal in the two phases.

Therefore, we write:

$$\left\| \left(\frac{\Delta\mu_1 - \Delta\mu_2}{RT(V_1 - V_2)} - \frac{\Delta\mu_3 - \Delta\mu_2}{RT(V_3 - V_2)} \right) \right\| = 0, \tag{14}$$

where $\|x\|$ denotes the difference in x over the two coexisting phases, and V_i is the molar volume of the component i. The steps involved in simplification of Eq. (14) are provided in Appendix B. Upon simplification and further mathematical rearrangements, we obtain

$$\Delta\left(\ln\frac{\Phi_1}{\Phi_3} - \left[\frac{V_1 - V_3}{V_2 - V_3}\right] \ln\frac{\Phi_2}{\Phi_3} \right) = \Delta(a), \tag{15}$$

where

$$\begin{aligned} a = \; & \chi_{12}\Phi_1 \left[(\Phi_1 + \Phi_3) - \frac{n_2(\Phi_2 + \Phi_3)}{n_1} - \frac{n_2\Phi_3(V_1 - V_2)}{n_3(V_3 - V_2)} \right. \\ & \left. - \frac{(\Phi_1 + \Phi_3)(V_1 - V_2)}{(V_3 - V_2)} \right] \\ & + \chi_{23}\Phi_3 \left[(\Phi_1 + \Phi_3) + \frac{n_2\Phi_1}{n_1} + \frac{n_2(\Phi_1 + \Phi_2)(V_1 - V_2)}{n_3(V_3 - V_2)} \right. \\ & \left. - \frac{(\Phi_1 + \Phi_3)(V_1 - V_2)}{(V_3 - V_2)} \right] \\ & + \chi_{13}\Phi_3 \left[-(\Phi_2 + \Phi_3) - \frac{n_1\Phi_2}{n_2} + \frac{n_1(\Phi_1 + \Phi_2)(V_1 - V_2)}{n_3(V_3 - V_2)} \right. \\ & \left. + \frac{n_1\Phi_2(V_1 - V_2)}{n_2(V_3 - V_2)} \right] \\ & + \left[(\Phi_1 - \Phi_2) - \frac{(n_1 + n_3)\Phi_2}{n_2} + \frac{(n_2 + n_3)\Phi_1}{n_1} + \frac{(\Phi_2 - \Phi_3)(V_1 - V_2)}{V_3 - V_2} \right. \\ & \left. - \frac{(n_1 + n_2)(V_1 - V_2)\Phi_3}{n_3(V_3 - V_2)} + \frac{(n_1 + n_3)(V_1 - V_2)\Phi_2}{n_2(V_3 - V_2)} \right] \\ & + fN \left[\frac{n_3\Phi_1}{n_1} - \frac{n_3\Phi_2}{n_2} + \frac{n_3\Phi_2(V_1 - V_2)}{n_2(V_3 - V_2)} + \frac{V_1 - V_2}{V_3 - V_2}\ln\Phi_3 \right] \\ & - \frac{\xi}{2} f^2 N \left[\frac{n_3\Phi_1}{n_1} - \frac{n_3\Phi_2}{n_2} + \frac{V_1 - V_2}{V_3 - V_2} \right. \\ & \left. \times \left(\Phi_1 + \Phi_2 + \ln(f\Phi_3) + \frac{n_3\Phi_2}{n_2} \right) \right]. \end{aligned} \tag{16}$$

From Eq. (16), it is evident that a is a collection of terms containing the χ parameters and the composition variables of the solution. For the purpose of estimating χ parameters, we use an approximation, wherein it is assumed that each cloud point represents a distinct phase composition. Then, if linear correlation has to necessarily occur between $\ln\frac{\Phi_1}{\Phi_3}$ and $\ln\frac{\Phi_2}{\Phi_3}$, as is known from experimental data, Eq. (15) implies that

$$\ln\frac{\Phi_1}{\Phi_3} - \left[\frac{V_1 - V_3}{V_2 - V_3}\right] \ln\frac{\Phi_2}{\Phi_3} = a \tag{17}$$

is valid for all cloud point occurrences. Therefore, a linear fit between $\ln\frac{\Phi_1}{\Phi_3}$ and $\ln\frac{\Phi_2}{\Phi_3}$ should ideally have a slope $\frac{V_1 - V_3}{V_2 - V_3}$ and intercept a.

Given the set of experimentally determined cloud point data at various solution compositions, Eq. (16) provides an overdetermined system of linear equations in the unknown variables χ_{23} and χ_{13}, with $\chi_{12}, a, f, \xi, N, \alpha, V_i, n_i$ and ϕ_i $(i = 1, 2, 3)$ being known quantities. Setting a and χ_{12} to the appropriate values determined in Sections 4.1 and 4.2.1, the molar volumes as ratio of molar mass to density, and other model parameters as in Table 3, the overdetermined system of equations was solved using a singular value decomposition method using the inbuilt svd command in MATLAB. The resulting values of χ_{23} and χ_{13} at the two temperatures are provided in Table 3.

The negative values for χ_{23} indicate strong affinity between NaPSS monomers and water molecules. This is expected due to the presence of ionized sulphonate groups of the NaPSS monomers that can favorably bind to the polar water molecules. Raghuram et al. [68] have shown through molecular dynamics simulations that water molecules, influenced by hydrogen bonding, order into multiple layers near the negatively charged sulphonate groups of NaPSS chains. Thus, NaPSS-water interactions are rendered favorable by the formation of multi-layered diffuse interphase of bound solvent molecules, particularly at temperatures close to or below room temperature. Though the layered arrangement prevails at higher temperatures, it is suggested that there is a reduction in the density of bound water molecules in the vicinity of sulphonate groups with increasing temperature, due to their migration to farther distances [68]. Moreover, at higher temperature, there would be a collapse of the polyion chains and desolvation of sodium ions, inducing stronger polyion–counterion interactions and weaker water–polyion interactions [69]. This is consistent with the reduced magnitude of χ_{23} obtained at 50 °C.

Although NaPSS–water interactions provide a favorable enthalpic contribution to mixing, there is an energy penalty for the polymer–non-solvent mixing that could induce local demixing in the ternary system, as indicated by positive values of χ_{13}. The unfavorable interaction between the polymer and non-solvent is due to the lower polarity of 1,4-butanediol, given its molecular symmetry and lower dielectric constant. The reduction in permittivity also causes counterion condensation on the polyion chains, promoting phase separation [69]. At 50 °C, χ_{13} has a small positive value. It may be inferred that 1,4-butanediol is nearly neutral to mixing with NaPSS at 50 °C purely by internal energy-based enthalpic considerations. However, this is offset by the reduced magnitudes of the negative χ_{23} and χ_{12} at 50 °C, resulting in a lower net magnitude of the FH enthalpy term. This is demonstrated in Fig. 7, where individual contributions to the Gibbs energy of mixing at the two temperatures are illustrated.

The various contributions to the net Gibbs energy of mixing (in units of Boltzmann energy k_BT per lattice site) are plotted (Fig. 7) as a function of the polymer volume fraction Φ_3 for a fixed ratio of Φ_1: $\Phi_2 = 1 : 1$. The four individual contributions arise from Flory–Huggins based random configurational entropy, Flory–Huggins type enthalpy stemming from internal energy-based short range interactions, counterion entropy, and the electrostatic interaction energy. The expression for the intensive property $\Delta G_{m,l}$, i.e., Gibbs energy of mixing per lattice site is provided in Appendix C. It is seen that bulk of the contributions to $\Delta G_{m,l}$ stem from FH entropy and FH enthalpy for the current system. Contributions from counterion entropy and electrostatic energy are rather small at the two temperatures. The electrostatic contribution will become more prominent in polyelectrolytes of smaller axial spacing between charged groups [67] (as it would increase ξ) and in systems with larger fraction of free counterions. In the presence of added salt, electrostatic repulsion between charges along the polyelectrolyte backbone may be weakened due to the shielding effect of the salt ions. Consequently, the polyelectrolyte chains would adopt more compact conformations compared to the extended conformations observed in salt-free solutions [72]. Therefore, phase separation can be promoted above a threshold salt concentration [73]. However, it also appears that there is a second threshold salt concentration above which the phase-separated precipitates can be made to redissolve due to screening of the electrostatic bridging attraction. Additionally, the contribution from mixing entropy term to the Gibbs energy will become more prominent in the presence of co-ions from added salts [30], enhancing the mixture compatibility, which would possibly cause the demixing region in the phase diagram to be narrower.

It may be noted that, as pointed out earlier (Section 2.2), the net Gibbs energy of mixing being negative is not a sufficient condition for the existence of a single phase homogeneous mixture. The shapes of derivatives of $\Delta G_{m,l}$, which are contained in the chemical potential and curvature, would determine phase separation. The shape of $\Delta G_{m,l}$ plotted in Fig. 7 is found to be similar at 25 °C and 50 °C. This is also consistent with similar shape of cloud point curves at the two temperatures in Fig. 4. We have also computed and plotted the spinodal

Table 3
Estimates of various quantities used in the model at 25 °C and 50 °C.

Quantity	25 °C	50 °C	Remarks
Average volume % of 1,4-butanediol in the liquid medium	55.3	53.8	Computed from the composition range over which the cloud point data was obtained experimentally. The relative volume fraction of 1,4-butanediol in the liquid medium of water + 1,4-butanediol varied over a narrow range of 50% – 60% in the entire cloud point data.
Dielectric constant of 1,4-butanediol	31.633	25.86	Gilani et al. [70] have measured and reported the dielectric constant of 1,4-butanediol at 25, 35, and 45 °C. Linear extrapolation of these values was used to estimate the dielectric constant at 50 °C.
Dielectric constant of water	78.3	69.9	Taken from Malmberg and Maryott [71].
Dielectric constant of mixture of water and 1,4-butanediol	52.5	46.2	Estimated through weighted average of the individual dielectric constants of water and 1,4-butanediol based on the average volume % of each liquid in the mixture.
Charge density parameter ξ	4.25	4.45	Estimated using the information that $\xi = 2.85$ for purely aqueous solutions of NaPSS at 25 °C and ξ is inversely proportional to the dielectric constant as well as temperature [67].
Fraction of free counterions f	0.23	0.24	Estimated using the information that f is inversely proportional to ξ and $f = 0.35$ for $\xi = 2.85$ (Ref. [67])
Degree of polymerization N	340	340	Average molar mass of polymer (70,000) divided by the molecular weight of repeating unit (206)
χ_{23}	−0.996	−0.720	Obtained by solving equation (16) using singular value decomposition method and cloud point data.
χ_{13}	+0.238	+0.042	

curve at the two temperatures, which depends on the second derivative of $\Delta G_{m,l}$ with respect to composition. Details are provided in section S2 of supplementary material. It may be seen that the spinodal curves have similar shape, but the demixing region at 50 °C is comparatively narrower than the one at 25 °C, suggesting enhanced stability of the mixture at higher temperature.

5. Conclusions

A simple and effective approach based on non-solvent induced cloud point titration has been demonstrated for determining phase equilibria in polyelectrolyte systems. NaPSS – water was used as a model polymer–solvent system with 1,4-butanediol as the non-solvent. The extrapolated cloud point curve of the ternary system, plotted using LCP curve correlations, depicts a tangible demixing region. The cloud point curves were found to be not significantly different at the two temperatures of investigation, viz. 25 °C and 50 °C. The binary FH interaction parameter for NaPSS – water system was estimated to be −0.996 and −0.720 at 25 °C and 50 °C respectively, in agreement with the affinity of water for NaPSS as a good solvent, and consistent with the theory of hydrogen bond induced solvent ordering around sulphonate groups of NaPSS [68].

The detailed mathematical model developed here through a combination of LCP approach and the extended FH equation would serve as a handy approach for easy determination of miscibility gaps and phase boundaries in other polyelectrolyte systems and ionic liquids. The model presented here could be refined further by incorporating non-random entropy contributions from the counterions and charged polymer groups, and by considering partially dissociated NaPSS as a true copolymer made up of charged and uncharged groups with different interaction parameters [67]. The results obtained for the specific model system considered here could provide useful insights for applications such as phase inversion for membrane fabrication [63], nano-precipitation for drug delivery [74,75], and polyelectrolyte coacervation [76].

CRediT authorship contribution statement

Rinsha Padmarajan: Methodology, Software, Investigation, Resources, Formal analysis, Data curation, Writing – original draft. **Sreeram K. Kalpathy:** Conceptualization, Methodology, Formal analysis, Writing – review & editing, Project administration, Supervision, Resources, Funding acquisition.

Declaration of competing interest

The authors declare that they have no known competing financial interests or personal relationships that could have appeared to influence the work reported in this paper.

Data availability

Data will be made available on request.

Acknowledgments

The authors thank P.G. Senapathy Computing Center, IIT Madras for access to computational resources, as well as Profs. K. C. Hari Kumar and Ethayaraja Mani for valuable discussions and insights.

Appendix A. Evaluation of derivatives $\partial \Phi_i / \partial n_i$

The derivatives of Φ_i's with respect to n_i's ($i = 1, 2, 3$) can be evaluated by differentiation of (2). The resulting expressions are:

$$\frac{\partial \Phi_1}{\partial n_1} = \frac{\Phi_1(\Phi_2 + \Phi_3)}{n_1}; \qquad \frac{\partial \Phi_2}{\partial n_1} = -\frac{\Phi_1 \Phi_2}{n_1}; \qquad \frac{\partial \Phi_3}{\partial n_1} = -\frac{\Phi_1 \Phi_3}{n_1}; \tag{A.1}$$

$$\frac{\partial \Phi_1}{\partial n_2} = -\frac{\Phi_1 \Phi_2}{n_2}; \qquad \frac{\partial \Phi_2}{\partial n_2} = \frac{\Phi_2(\Phi_1 + \Phi_3)}{n_2}; \qquad \frac{\partial \Phi_3}{\partial n_2} = -\frac{\Phi_2 \Phi_3}{n_2}; \tag{A.2}$$

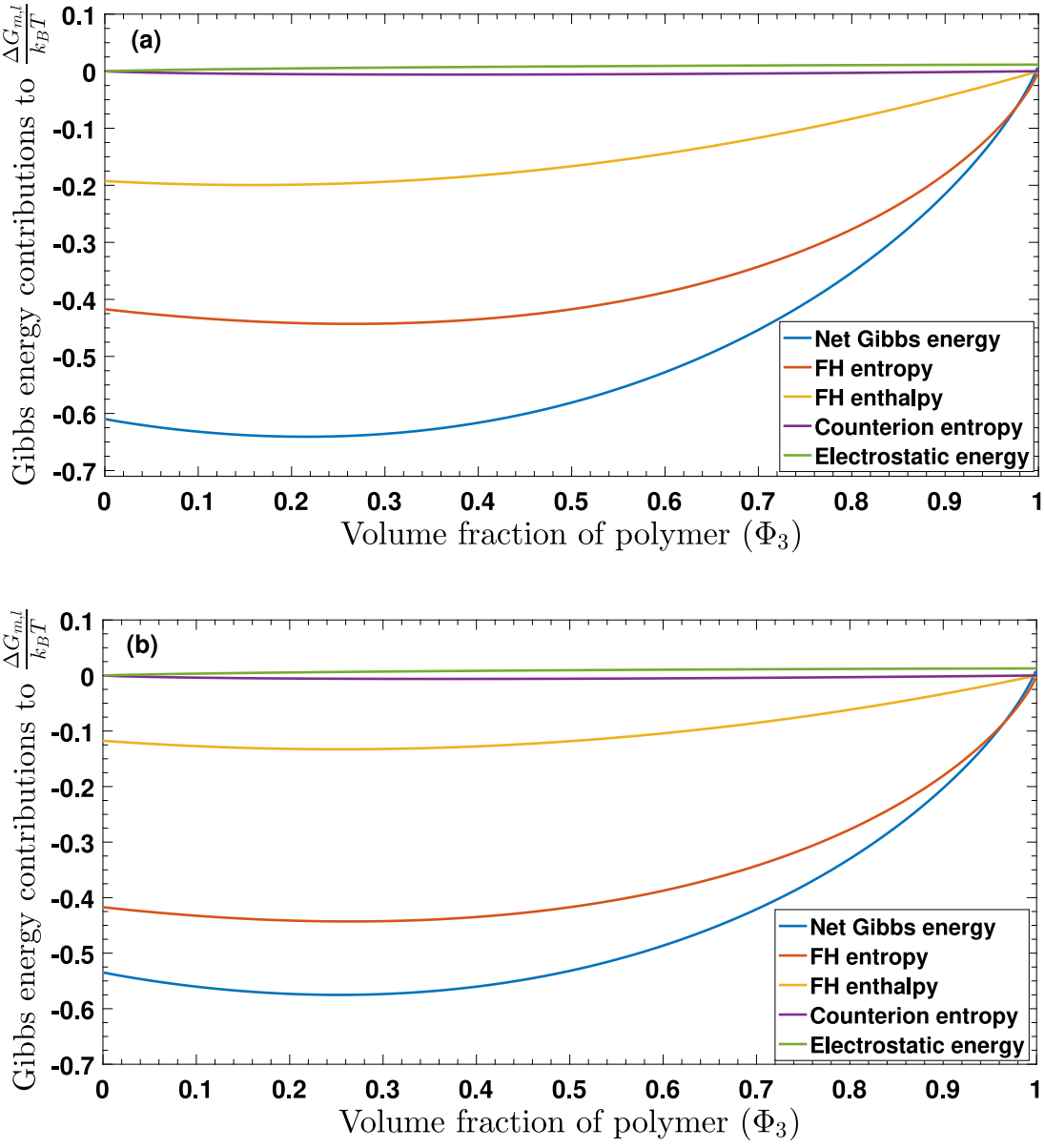

Fig. 7. Various contributions to the net Gibbs energy of mixing as function of the polymer volume fraction at (a) 25 °C, (b) at 50 °C for solvent:non-solvent volume ratio of 1:1.

$$\frac{\partial \Phi_1}{\partial n_3} = -\frac{\Phi_1 \Phi_3}{n_3}; \qquad \frac{\partial \Phi_2}{\partial n_3} = -\frac{\Phi_2 \Phi_3}{n_3}; \qquad \frac{\partial \Phi_3}{\partial n_3} = \frac{(\Phi_1 + \Phi_2)\Phi_3}{n_3}. \tag{A.3}$$

Appendix B. Simplification of Eq. (14) to arrive at eq. (15)

Using the expressions (10), (11), (12) for chemical potentials $\Delta\mu_i$ ($i = 1, 2, 3$), we get the following.

$$\begin{aligned}\frac{(\Delta\mu_1 - \Delta\mu_2)}{(V_1 - V_2)RT} =& \frac{1}{(V_1 - V_2)} \ln\frac{\Phi_1}{\Phi_2} + \frac{\Phi_2 - \Phi_1}{V_1 - V_2} + \frac{(n_1 + n_3)\Phi_2}{n_2(V_1 - V_2)} - \frac{(n_2 + n_3)\Phi_1}{(V_1 - V_2)n_1} \\ &+ \frac{\chi_{12}\Phi_1}{V_1 - V_2}\left[\frac{n_2}{n_1}(\Phi_2 + \Phi_3) - (\Phi_1 + \Phi_3)\right] \\ &- \frac{\chi_{23}\Phi_3}{V_1 - V_2}\left[\frac{n_2}{n_1}\Phi_1 + (\Phi_1 + \Phi_3)\right] \\ &+ \frac{\chi_{13}\Phi_3}{V_1 - V_2}\left[\frac{n_1}{n_2}\Phi_2 + (\Phi_2 + \Phi_3)\right] \\ &+ \frac{\alpha}{V_1 - V_2}\left[\frac{n_3}{n_2}\Phi_2 - \frac{n_3}{n_1}\Phi_1\right] \\ &+ \frac{\xi}{2} f^2 N\left(\frac{1}{V_1 - V_2}\right)\left[\frac{n_3}{n_1}\Phi_1 - \frac{n_3}{n_2}\Phi_2\right]; \end{aligned} \tag{B.1}$$

$$\begin{aligned}\frac{(\Delta\mu_3 - \Delta\mu_2)}{(V_3 - V_2)RT} =& \frac{1}{(V_3 - V_2)} \ln\frac{\Phi_3}{\Phi_2} + \frac{\Phi_2 - \Phi_3}{V_3 - V_2} + \frac{(n_1 + n_3)\Phi_2}{n_2(V_3 - V_2)} - \frac{(n_1 + n_2)\Phi_3}{(V_3 - V_2)n_3} \\ &- \frac{\chi_{12}\Phi_1}{V_3 - V_2}\left[\frac{n_2\Phi_3}{n_3} + (\Phi_1 + \Phi_3)\right] \\ &+ \frac{\chi_{23}\Phi_3}{V_3 - V_2}\left[\frac{n_2}{n_3}(\Phi_1 + \Phi_2) - (\Phi_1 + \Phi_3)\right] \\ &+ \frac{\chi_{13}\Phi_3}{V_3 - V_2}\left[\frac{n_1}{n_3}(\Phi_1 + \Phi_2) + \frac{n_1}{n_2}(\Phi_2)\right] \\ &+ \frac{\alpha}{V_3 - V_2}\left[(\Phi_1 + \Phi_2) + \ln\Phi_3 + \frac{n_3}{n_2}\Phi_2\right] \\ &- \frac{\xi}{2} f^2 N\left(\frac{1}{V_3 - V_2}\right)\left[(\Phi_1 + \Phi_2) + \ln(f\Phi_3) + \frac{n_3}{n_2}\Phi_2\right]. \end{aligned} \tag{B.2}$$

By performing the subtraction of (B.2) from (B.1), the left hand side (LHS) of (14) can be evaluated to be equal to:

$$
\begin{aligned}
&\Delta\left(\frac{1}{V_1-V_2}\ln\frac{\Phi_1}{\Phi_2}-\frac{1}{V_3-V_2}\ln\frac{\Phi_3}{\Phi_2}\right)\\
&+\Delta\Bigg(-\chi_{12}\Phi_1\left[\frac{\Phi_1+\Phi_3}{V_1-V_2}-\frac{n_2(\Phi_2+\Phi_3)}{n_1(V_1-V_2)}-\frac{n_2\Phi_3}{n_3(V_3-V_2)}-\frac{(\Phi_1+\Phi_3)}{(V_3-V_2)}\right]\\
&\quad-\chi_{23}\Phi_3\left[\frac{\Phi_1+\Phi_3}{V_1-V_2}+\frac{n_2\Phi_1}{n_1(V_1-V_2)}+\frac{n_2(\Phi_1+\Phi_2)}{n_3(V_3-V_2)}-\frac{(\Phi_1+\Phi_3)}{(V_3-V_2)}\right]\\
&\quad-\chi_{13}\Phi_3\left[-\frac{\Phi_2+\Phi_3}{V_1-V_2}-\frac{n_1\Phi_2}{n_2(V_1-V_2)}+\frac{n_1(\Phi_1+\Phi_2)}{n_3(V_3-V_2)}+\frac{n_1\Phi_2}{n_2(V_3-V_2)}\right]\\
&\quad-\left[\frac{\Phi_1-\Phi_2}{V_1-V_2}-\frac{(n_1+n_3)\Phi_2}{n_2(V_1-V_2)}+\frac{(n_2+n_3)\Phi_1}{n_1(V_1-V_2)}+\frac{(\Phi_2-\Phi_3)}{V_3-V_2}\right.\\
&\qquad\left.-\frac{(n_1+n_2)\Phi_3}{n_3(V_3-V_2)}+\frac{(n_1+n_3)\Phi_2}{n_2(V_3-V_2)}\right]\\
&\quad+\alpha\left[\frac{n_3\Phi_2}{n_2(V_1-V_2)}-\frac{n_3\Phi_1}{n_1(V_1-V_2)}-\frac{\Phi_1+\Phi_2+\ln\Phi_3}{(V_3-V_2)}-\frac{n_3\Phi_2}{n_2(V_3-V_2)}\right]\\
&\quad+\frac{\xi}{2}f^2N\left[\frac{n_3\Phi_1}{n_1(V_1-V_2)}-\frac{n_2\Phi_2}{n_2(V_1-V_2)}+\frac{(\Phi_1+\Phi_2)+\ln(f\Phi_3)}{(V_3-V_2)}\right.\\
&\qquad\left.+\frac{n_3\Phi_2}{n_2(V_3-V_2)}\right]\Bigg).
\end{aligned}
\tag{B.3}
$$

Now, Eq. (B.3), when multiplied by (V_1-V_2), followed by some rearrangements, will yield (15). The steps involved are described below.

The first term in (B.3) containing the logarithms, i.e., $\Delta\left(\frac{1}{V_1-V_2}\ln\frac{\Phi_1}{\Phi_2}-\frac{1}{V_3-V_2}\ln\frac{\Phi_3}{\Phi_2}\right)$, when multiplied by (V_1-V_2), can be written as

$$
\Delta\left(\ln\frac{\Phi_1}{\Phi_2}-\frac{V_1-V_2}{V_3-V_2}\ln\frac{\Phi_3}{\Phi_2}\right).
\tag{B.4}
$$

Given that $\frac{V_1-V_2}{V_3-V_2}=1-\frac{V_1-V_3}{V_2-V_3}$, it can be easily shown that (B.4) is equal to:

$$
\Delta\left(\ln\frac{\Phi_1}{\Phi_3}-\frac{V_1-V_3}{V_3-V_2}\ln\frac{\Phi_2}{\Phi_3}\right).
\tag{B.5}
$$

It can be easily verified that the second, bigger term of (B.3), when multiplied by (V_1-V_2), is equal to $\Delta(-a)$, where a is as defined in (16). Therefore, the LHS of (14) now becomes:

$$
\Delta\left(\ln\frac{\Phi_1}{\Phi_3}-\frac{V_1-V_3}{V_3-V_2}\ln\frac{\Phi_2}{\Phi_3}\right)-\Delta(a).
\tag{B.6}
$$

Since the expression in (B.6) is equal to zero as per (14), we have

$$
\Delta\left(\ln\frac{\Phi_1}{\Phi_3}-\left[\frac{V_1-V_3}{V_2-V_3}\right]\ln\frac{\Phi_2}{\Phi_3}\right)=\Delta(a),
\tag{B.7}
$$

which is the same as (15).

Appendix C. Expression for $\Delta G_{m,l}/k_BT$ used in Fig. 7

Eq. (2) may be rearranged as:

$$
n_i=\frac{\Phi_i}{V_i}\sum_{i=1}^{3}n_iV_i.
\tag{C.1}
$$

The total number of lattice sites is equal to the total volume of all molecules divided by the volume of one lattice site. Assuming that a molecule of the solvent, water, being small, occupies the volume of one lattice site, the number of lattice sites is equal to $N_{AV}\sum_{i=1}^{3}(n_iV_i)/V_2$, where N_{AV} is the Avogadro number. Eq. (9) can be divided by the number of lattice sites to obtain $\Delta G_{m,l}$. Noting that $R=N_{AV}k_B$, and by replacing n_i in terms of Φ_i using (C.1), we obtain

$$
\begin{aligned}
\frac{\Delta G_{m,l}}{k_BT}&=\frac{\Phi_1\ln\Phi_1}{V_1/V_2}+\Phi_2\ln\Phi_2+\frac{\Phi_3(1+\alpha)\ln\Phi_3}{V_3/V_2}+\Phi_2\Phi_1\chi_{12}+\Phi_2\Phi_3\chi_{23}\\
&\quad+\frac{\Phi_1\Phi_3\chi_{13}}{V_1/V_2}-\frac{\xi f^2N\Phi_3\ln(f\Phi_3)}{2V_3/V_2}.
\end{aligned}
\tag{C.2}
$$

Appendix D. Supplementary data

Supplementary material related to this article can be found online at https://doi.org/10.1016/j.fluid.2023.113935. Supplementary material includes experimental data in tabular form.

References

[1] Fei Wang, Patrick Altschuh, Lorenz Ratke, Haodong Zhang, Michael Selzer, Britta Nestler, Progress report on phase separation in polymer solutions, Adv. Mater. 31 (26) (2019) 1806733, http://dx.doi.org/10.1002/adma.201806733.

[2] A.R. Shultz, P.J. Flory, Phase equilibria in polymer—solvent systems - 1, 2, J. Am. Chem. Soc. 74 (19) (1952) 4760–4767, http://dx.doi.org/10.1021/ja01139a010.

[3] Pratchaya Tipduangta, Peter Belton, Laszlo Fabian, Li Ying Wang, Huiru Tang, Mark Eddleston, Sheng Qi, Electrospun polymer blend nanofibers for tunable drug delivery: the role of transformative phase separation on controlling the release rate, Mol. Pharmaceut. 13 (1) (2016) 25–39, http://dx.doi.org/10.1021/acs.molpharmaceut.5b00359.

[4] Seema Thakral, Naveen K. Thakral, Prediction of drug–polymer miscibility through the use of solubility parameter based Flory–Huggins interaction parameter and the experimental validation: PEG as model polymer, J. Pharm. Sci. 102 (7) (2013) 2254–2263, http://dx.doi.org/10.1002/jps.23583.

[5] Catharina Kahrs, Thorben Gühlstorf, Jan Schwellenbach, Influences of different preparation variables on polymeric membrane formation via nonsolvent induced phase separation, J. Appl. Polym. Sci. 137 (28) (2020) 48852, http://dx.doi.org/10.1002/app.48852.

[6] Xiaobo Dong, Tae J Jeong, Eric Kline, Lillian Banks, Eric Grulke, Tequila Harris, Isabel C Escobar, Eco-friendly solvents and their mixture for the fabrication of polysulfone ultrafiltration membranes: An investigation of doctor blade and slot die casting methods, J. Membr. Sci. 614 (2020) 118510, http://dx.doi.org/10.1016/j.memsci.2020.118510.

[7] Shichen Li, Bong-Kee Lee, Morphological development of immersion-electrospun polymer products based on nonsolvent-induced phase separation, ACS Appl. Polym. Mater. 4 (2) (2022) 879–888, http://dx.doi.org/10.1021/acsapm.1c01374.

[8] Yabing Tang, Baojun Lin, Hanzhang Zhao, Tao Li, Wei Ma, Han Yan, Significance of dopant/component miscibility to efficient N-doping in polymer solar cells, ACS Appl. Mater. Interfaces 12 (11) (2020) 13021–13028, http://dx.doi.org/10.1021/acsami.9b21252.

[9] Li Chen, Andre Bertolini, Francois Dubost, Vladislav Achourov, Soraya Betancourt, Jesus A Cañas, Hadrien Dumont, Andrew E Pomerantz, Oliver C Mullins, Yen–mullins model applies to oilfield reservoirs, Energy Fuels 34 (11) (2020) 14074–14093, http://dx.doi.org/10.1021/acs.energyfuels.0c02937.

[10] Kamalika Roy, Susanta Lahiri, Extraction of Hg (I), Hg (II) and methylmercury using polyethylene glycol based aqueous biphasic system, Appl. Radiat. Isot. 67 (10) (2009) 1781–1784, http://dx.doi.org/10.1016/j.apradiso.2009.05.018.

[11] Roberta de Almeida Carvalho, Jussara Alves Penido, Fabiana Aparecida Lobo, Poliana Aparecida Lopes Machado, Nelson Henrique Lemes Teixeira, Luciano Sindra Virtuoso, Leandro Rodrigues de Lemos, Guilherme Dias Rodrigues, Aparecida Barbosa Mageste, Thermodynamic investigation of the aqueous two-phase systems formed by PEG 400+ water+ either sodium carbonate or potassium carbonate at different temperatures: experimental and correlational approaches, J. Chem. Eng. Data 64 (2) (2019) 448–458, http://dx.doi.org/10.1021/acs.jced.8b00546.

[12] Hermínio C. De Sousa, Luís P.N. Rebelo, A continuous polydisperse thermodynamic algorithm for a modified flory–huggins model: The (polystyrene+ nitroethane) example, J. Polym. Sci. B: Polym. Phys. 38 (4) (2000) 632–651, http://dx.doi.org/10.1002/(SICI)1099-0488(20000215)38:4<632::AID-POLB15>3.0.CO;2-Q.

[13] Paul J. Flory, Thermodynamics of high polymer solutions, J. Chem. Phys. 10 (1) (1942) 51–61, http://dx.doi.org/10.1063/1.1723621.

[14] Paul J. Flory, Principles of Polymer Chemistry, Cornell University Press, 1953.

[15] Maurice L. Huggins, Theory of solutions of high polymers - 1, J. Am. Chem. Soc. 64 (7) (1942) 1712–1719, http://dx.doi.org/10.1021/ja01259a068.

[16] Isaac C. Sanchez, Robert H. Lacombe, Statistical thermodynamics of polymer solutions, Macromolecules 11 (6) (1978) 1145–1156, http://dx.doi.org/10.1021/ma60066a017.

[17] Ioannis G. Economou, Statistical associating fluid theory: A successful model for the calculation of thermodynamic and phase equilibrium properties of complex fluid mixtures, Ind. Eng. Chem. Res. 41 (5) (2002) 953–962, http://dx.doi.org/10.1021/ie0102201.

[18] C.J. Sheehan, A.L. Bisio, Polymer/solvent interaction parameters, Rubber Chem. Technol. 39 (1) (1966) 149–192, http://dx.doi.org/10.5254/1.3544827.

[19] William W Graessley, Ramanan Krishnamoorti, Nitash P Balsara, Lewis J Fetters, David J Lohse, Donald N Schulz, Joseph A Sissano, Deuteration effects and solubility parameter ordering in blends of saturated hydrocarbon polymers, Macromolecules 27 (9) (1994) 2574–2579, http://dx.doi.org/10.1021/ma00087a028.

[20] Yang Liu, Baoli Shi, Determination of flory interaction parameters between polyimide and organic solvents by HSP theory and IGC, Polym. Bull. 61 (2008) 501–509, http://dx.doi.org/10.1007/s00289-008-0963-1.
[21] Tomoo Shiomi, Katsumi Kohno, Kohji Yoneda, Tetsuo Tomita, Masamitsu Miya, Kiyokazu Imai, Thermodynamic interactions in the poly (vinyl methyl ether)-polystyrene system, Macromolecules 18 (3) (1985) 414–419, http://dx.doi.org/10.1021/ma00145a020.
[22] P.T.P. Aryanti, D. Ariono, A.N. Hakim, I.G. Wenten, Flory-huggins based model to determine thermodynamic property of polymeric membrane solution, in: Journal of Physics: Conference Series, Vol. 1090, IOP Publishing, 2018, 012074, http://dx.doi.org/10.1088/1742-6596/1090/1/012074.
[23] K. Ito, J.E. Guillet, Estimation of solubility parameters for some olefin polymers and copolymers by inverse gas chromatography, Macromolecules 12 (6) (1979) 1163–1167, http://dx.doi.org/10.1021/ma60072a030.
[24] Paul C. Hiemenz, Timothy P. Lodge, Polymer Chemistry, CRC Press, 2007.
[25] Takeshi Fukuda, Minoru Nagata, Hiroshi Inagaki, Light scattering from ternary solutions. 1. Dilute solutions of polystyrene and poly (methyl methacrylate), Macromolecules 17 (4) (1984) 548–553, http://dx.doi.org/10.1021/ma00134a007.
[26] Alexander P Safronov, Felix A Blyakhman, Tatyana F Shklyar, Tatyana V Terziyan, Marina A Kostareva, Sergey A Tchikunov, Gerald H Pollack, The influence of counterion type and temperature on flory-huggins binary interaction parameter in polyelectrolyte hydrogels, Macromol. Chem. Phys. 210 (7) (2009) 511–519, http://dx.doi.org/10.1002/macp.200800495.
[27] Sarah L. Perry, Charles E. Sing, Prism-based theory of complex coacervation: Excluded volume versus chain correlation, Macromolecules 48 (14) (2015) 5040–5053, http://dx.doi.org/10.1021/acs.macromol.5b01027.
[28] Michael Beckinghausen, Andrew J. Spakowitz, Interplay of polymer structure, solvent ordering, and charge fluctuations in polyelectrolyte solution thermodynamics, Macromolecules (2022) http://dx.doi.org/10.1021/acs.macromol.2c01826.
[29] Laise Maia Lopes, Mariana Agostini De Moraes, Marisa Masumi Beppu, Phase diagram and estimation of flory-huggins parameter of interaction of silk fibroin/sodium alginate blends, Front. Bioeng. Biotechnol. 8 (2020) 973, http://dx.doi.org/10.3389/fbioe.2020.00973.
[30] Ha-Kyung Kwon, Jos W Zwanikken, Kenneth R Shull, Monica Olvera de la Cruz, Theoretical analysis of multiple phase coexistence in polyelectrolyte blends, Macromolecules 48 (16) (2015) 6008–6015, http://dx.doi.org/10.1021/acs.macromol.5b00901.
[31] Stig Hellebust, Svante Nilsson, Anne Marit Blokhus, Phase behavior of anionic polyelectrolyte mixtures in aqueous solution. effects of molecular weights, polymer charge density, and ionic strength of solution, Macromolecules 36 (14) (2003) 5372–5382, http://dx.doi.org/10.1021/ma021442t.
[32] Lawrence Scherr, David A Ogden, Allen W Mead, Norton Spritz, Albert L Rubin, Management of hyperkalemia with a cation-exchange resin, N. Engl. J. Med. 264 (3) (1961) 115–119, http://dx.doi.org/10.1056/NEJM196101192640303.
[33] Mario V. Beccari, Calvin J. Meaney, Clinical utility of patiromer, sodium zirconium cyclosilicate, and sodium polystyrene sulfonate for the treatment of hyperkalemia: an evidence-based review, Core Evidence 12 (2017) 11, http://dx.doi.org/10.2147/CE.S129555.
[34] Gil Chernin, Amir Gal-Oz, Eyal Ben-Assa, Idit F Schwartz, Talia Weinstein, Doron Schwartz, Donald S Silverberg, Secondary prevention of hyperkalemia with sodium polystyrene sulfonate in cardiac and kidney patients on renin-angiotensin-aldosterone system inhibition therapy, Clin. Cardiol. 35 (1) (2012) 32–36, http://dx.doi.org/10.1002/clc.20987.
[35] Chad Kessler, Jaclyn Ng, Kathya Valdez, Hui Xie, Brett Geiger, The use of sodium polystyrene sulfonate in the inpatient management of hyperkalemia, J. Hosp. Med. 6 (3) (2011) 136–140, http://dx.doi.org/10.1002/jhm.834.
[36] Alan Soares Landim, Guimes Rodrigues Filho, Rosana Maria Nascimento de Assunção, Use of polystyrene sulfonate produced from waste plastic cups as an auxiliary agent of coagulation, flocculation and flotation for water and wastewater treatment in municipal department of water and wastewater in Uberlândia-MG, Brazil, Polym. Bull. 58 (2) (2007) 457–463, http://dx.doi.org/10.1007/s00289-006-0669-1.
[37] Nicola Di Trani, Antonia Silvestri, Antons Sizovs, Yu Wang, Donald R Erm, Danilo Demarchi, Xuewu Liu, Alessandro Grattoni, Electrostatically gated nanofluidic membrane for ultra-low power controlled drug delivery, Lab Chip 20 (9) (2020) 1562–1576, http://dx.doi.org/10.1039/D0LC00121J.
[38] Guichen Zhou, Ying Lu, He Zhang, Yan Chen, Yuan Yu, Jing Gao, Duxin Sun, Guoqing Zhang, Hao Zou, Yanqiang Zhong, A novel pulsed drug-delivery system: polyelectrolyte layer-by-layer coating of chitosan–alginate microgels, Int. J. Nanomedicine 8 (2013) 877, http://dx.doi.org/10.2147/IJN.S38144.
[39] Stephan Kirchmeyer, Knud Reuter, Scientific importance, properties and growing applications of poly (3, 4-ethylenedioxythiophene), J. Mater. Chem. 15 (21) (2005) 2077–2088, http://dx.doi.org/10.1039/B417803N.
[40] Lambertus Groenendaal, Friedrich Jonas, Dieter Freitag, Harald Pielartzik, John R Reynolds, Poly (3, 4-ethylenedioxythiophene) and its derivatives: past, present, and future, Adv. Mater. 12 (7) (2000) 481–494, http://dx.doi.org/10.1002/(SICI)1521-4095(200004)12:7<481::AID-ADMA481>3.0.CO;2-C.
[41] Dawn T. Eriksen, Sijin Li, Huimin Zhao, Pathway engineering as an enabling synthetic biology tool, in: Synthetic Biology, Wiley, 2013, pp. 43–61, http://dx.doi.org/10.1016/B978-0-12-394430-6.00003-0.
[42] Vitaly J. Klenin, Sergei L. Shmakov, Features of phase separation in polymeric systems: cloud-point curves (discussion), Univ. J. Mater. Sci. 1 (2) (2013) 39–45, http://dx.doi.org/10.13189/ujms.2013.010205.
[43] J.G. Wijmans, J. Kant, M.H.V. Mulder, C.A. Smolders, Phase separation phenomena in solutions of polysulfone in mixtures of a solvent and a nonsolvent: relationship with membrane formation, Polymer 26 (10) (1985) 1539–1545, http://dx.doi.org/10.1016/0032-3861(85)90090-4.
[44] Alberto Arce, Alberto Arce Jr., Oscar Rodriguez, Revising concepts on liquid–liquid extraction: data treatment and data reliability, J. Chem. Eng. Data 67 (1) (2021) 286–296, http://dx.doi.org/10.1021/acs.jced.1c00778.
[45] RM Boom, Th Van den Boomgaard, JWA Van den Berg, CA Smolders, Linearized cloudpoint curve correlation for ternary systems consisting of one polymer, one solvent and one non-solvent, Polymer 34 (11) (1993) 2348–2356, http://dx.doi.org/10.1016/0032-3861(93)90819-V.
[46] J.H. Hildebrand, A history of solution theory, Annu. Rev. Phys. Chem. 32 (1) (1981) 1–24, http://dx.doi.org/10.1146/annurev.pc.32.100181.000245.
[47] AMW Bulte, EM Naafs, F Van Eeten, MHV Mulder, CA Smolders, H Strathmann, Equilibrium thermodynamics of the ternary membrane-forming system nylon, formic acid and water, Polymer 37 (9) (1996) 1647–1655, http://dx.doi.org/10.1016/0032-3861(96)83714-1.
[48] Chi-Lun Lee, Murugappan Muthukumar, Phase behavior of polyelectrolyte solutions with salt, J. Chem. Phys. 130 (2) (2009) 01B608, http://dx.doi.org/10.1063/1.3054140.
[49] Patrick B. Warren, Simplified mean field theory for polyelectrolyte phase behaviour, J. Phys. II 7 (2) (1997) 343–361, http://dx.doi.org/10.1051/jp2:1997129.
[50] A.R. Khokhlov, I.A. Nyrkova, Compatibility enhancement and microdomain structuring in weakly charged polyelectrolyte mixtures, Macromolecules 25 (5) (1992) 1493–1502, http://dx.doi.org/10.1021/ma00031a021.
[51] Michael Gottschalk, Per Linse, Lennart Piculell, Phase stability of polyelectrolyte solutions as predicted from lattice mean-field theory, Macromolecules 31 (23) (1998) 8407–8416, http://dx.doi.org/10.1021/ma980866d.
[52] L Piculell, I Illiopoulos, P Linse, S Nilsson, T Turquois, C Viebke, W Zhang, Gums and Stabilisers for the Food Industry 6, Oxford Univ. Press, Oxford, 1994, p. 309.
[53] Gerald S. Manning, Limiting laws and counterion condensation in polyelectrolyte solutions I. Colligative properties, J. Chem. Phys. 51 (3) (1969) 924–933, http://dx.doi.org/10.1063/1.1672157.
[54] M. Yu, J. de Swaan Arons, Phase behaviour of aqueous solutions of neutral and charged polymer mixtures, Polymer 35 (16) (1994) 3499–3502, http://dx.doi.org/10.1016/0032-3861(94)90915-6.
[55] Gerald S. Manning, Counterion binding in polyelectrolyte theory, Acc. Chem. Res. 12 (12) (1979) 443–449, http://dx.doi.org/10.1021/ar50144a004.
[56] Saskia Lindhoud, Willem Norde, Martien A. Cohen Stuart, Reversibility and relaxation behavior of polyelectrolyte complex micelle formation, J. Phys. Chem. B 113 (16) (2009) 5431–5439, http://dx.doi.org/10.1021/jp809489f.
[57] Tommy Nylander, Yulia Samoshina, Björn Lindman, Formation of polyelectrolyte–surfactant complexes on surfaces, Adv. Colloid Interface Sci. 123 (2006) 105–123, http://dx.doi.org/10.1016/j.cis.2006.07.005.
[58] Ludwik Leibler, Henri Orland, John C. Wheeler, Theory of critical micelle concentration for solutions of block copolymers, J. Chem. Phys. 79 (7) (1983) 3550–3557, http://dx.doi.org/10.1063/1.446209.
[59] J. Barzin, B. Sadatnia, Theoretical phase diagram calculation and membrane morphology evaluation for water/solvent/polyethersulfone systems, Polymer 48 (6) (2007) 1620–1631, http://dx.doi.org/10.1016/j.polymer.2007.01.049.
[60] Yong-Ming Wei, Zhen-Liang Xu, Xiao-Tian Yang, Hong-Lai Liu, Mathematical calculation of binodal curves of a polymer/solvent/nonsolvent system in the phase inversion process, Desalination 192 (1–3) (2006) 91–104, http://dx.doi.org/10.1016/j.desal.2005.07.035.
[61] L. Yilmaz, A.J. McHugh, Analysis of nonsolvent–solvent–polymer phase diagrams and their relevance to membrane formation modeling, J. Appl. Polym. Sci. 31 (4) (1986) 997–1018, http://dx.doi.org/10.1002/app.1986.070310404.
[62] Amin Ghasemi, Milad Asgarpour Khansary, Mohammad Ali Aroon, A comparative theoretical and experimental study on liquid-liquid equilibria of membrane forming polymeric solutions, Fluid Phase Equilib. 435 (2017) 60–72, http://dx.doi.org/10.1016/j.fluid.2016.12.005.
[63] Catharina Kahrs, Michael Metze, Christian Fricke, Jan Schwellenbach, Thermodynamic analysis of polymer solutions for the production of polymeric membranes, J. Mol. Liq. 291 (2019) 111351, http://dx.doi.org/10.1016/j.molliq.2019.111351.
[64] Gregory R. Guillen, Yinjin Pan, Minghua Li, Eric M.V. Hoek, Preparation and characterization of membranes formed by nonsolvent induced phase separation: a review, Ind. Eng. Chem. Res. 50 (7) (2011) 3798–3817, http://dx.doi.org/10.1021/ie101928r.
[65] S.J. Law, S.K. Mukhopadhyay, The construction of a phase diagram for a ternary system used for the wet spinning of acrylic fibers based on a linearized cloudpoint curve correlation, J. Appl. Polym. Sci. 65 (11) (1997) 2131–2139, http://dx.doi.org/10.1002/(SICI)1097-4628(19970912)65:11<2131::AID-APP9>3.0.CO;2-I.

[66] M.Y. Nagamachi, A.Z. Francesconi, Measurement and correlation of excess molar enthalpy HmE for (1, 2-propanediol, or 1, 3-propanediol, or 1, 4-butanediol+ water) at the temperatures 298.15, 323.15, and 343.15 K, J. Chem. Thermodyn. 38 (4) (2006) 461–466, http://dx.doi.org/10.1016/j.jct.2005.06.018.

[67] Markku Laatikainen, Ismo Markkanen, Jari Tiihonen, Erkki Paatero, Liquid–liquid equilibria in ternary systems of linear and cross-linked water-soluble polymers, Fluid Phase Equilib. 201 (2) (2002) 381–399, http://dx.doi.org/10.1016/S0378-3812(02)00078-X.

[68] E. Raghuram, Rinsha Padmarajan, Sreeram K. Kalpathy, Hydrogen bond induced solvent ordering in aqueous poly (sodium p-styrenesulfonate), Polymer 262 (2022) 125380, http://dx.doi.org/10.1016/j.polymer.2022.125380.

[69] Ons Zoghlami, Moez Guettari, Tahar Tajouri, Study of poly (sodium-4-styrenesulfonate) behavior in water/non-solvent mixtures by conductivity and refractive index measurements, Colloid Polym. Sci. 295 (9) (2017) 1729–1739, http://dx.doi.org/10.1007/s00396-017-4104-y.

[70] A. Ghanadzadeh Gilani, H. Ghanadzadeh Gilani, M. Ansari, A thermodynamic study of solute–solvent interactions through dielectric properties of the mixtures consisting of 1, 4-butanediol, 1-octanol, and 1, 4-dioxane at different temperatures, J. Chem. Thermodyn. 55 (2012) 203–212, http://dx.doi.org/10.1016/j.jct.2012.05.032.

[71] C.G. Malmberg, A.A. Maryott, Dielectric constant of water from 0 to 100 C, J. Res. Natl. Bureau Stand. 56 (1) (1956) 1–8, http://dx.doi.org/10.6028/JRES.056.001.

[72] Nicholas B. Wyatt, Casey M. Gunther, Matthew W. Liberatore, Increasing viscosity in entangled polyelectrolyte solutions by the addition of salt, Polymer 52 (11) (2011) 2437–2444, http://dx.doi.org/10.1016/j.polymer.2011.03.053.

[73] Pengfei Zhang, Nayef M Alsaifi, Jianzhong Wu, Zhen-Gang Wang, Salting-out and salting-in of polyelectrolyte solutions: A liquid-state theory study, Macromolecules 49 (24) (2016) 9720–9730, http://dx.doi.org/10.1021/acs.macromol.6b02160.

[74] Moritz Beck-Broichsitter, Solvent impact on polymer nanoparticles prepared nanoprecipitation, Colloids Surf. A 625 (2021) 126928, http://dx.doi.org/10.1016/j.colsurfa.2021.126928.

[75] Christiana E. Udoh, Valeria Garbin, Joao T. Cabral, Microporous polymer particles via phase inversion in microfluidics: Impact of nonsolvent quality, Langmuir 32 (32) (2016) 8131–8140, http://dx.doi.org/10.1021/acs.langmuir.6b01799.

[76] Srivastava S. Tirrell, Polyelectrolyte complexation, in: Advances in Chemical Physics, Vol. 161, Wiley, 2016, pp. 499–544, http://dx.doi.org/10.1002/9781119290971.ch7.